Applied Catalysis B: Environmental 89 (2009) 196–203

Contents lists available at ScienceDirect

Applied Catalysis B: Environmental

journal homepage: www.elsevier.com/locate/apcatb

Role of tetrahedral Co(II) sites of CoSiBEA zeolite in the selective catalytic reduction of NO: XRD, UV–vis, XAS and catalysis study

Janusz Janas [a,**], Tetsuya Shishido [b], Michel Che [c,d,e], Stanislaw Dzwigaj [c,d,*]

[a] Institute of Catalysis and Surface Chemistry, Polish Academy of Sciences, Niezapominajek 8, 30239 Krakow, Poland
[b] Department of Molecular Engineering, Graduate School of Engineering, Kyoto University, Kyoto, 615-8510, Japan
[c] UPMC Univ Paris 6, UMR 7609, Laboratoire de Réactivité de Surface, 4 Place Jussieu, 75252 Paris Cedex 05, France
[d] CNRS, UMR 7609, Laboratoire de Réactivité de Surface, 4 Place Jussieu, 75252 Paris Cedex 05, France
[e] Institut Universitaire de France, France

ARTICLE INFO

Article history:
Received 18 September 2008
Received in revised form 21 November 2008
Accepted 22 November 2008
Available online 27 November 2008

Keywords:
SiBEA zeolite
Cobalt
SCR
NO
Ethanol
XRD
FTIR
DR UV–vis
XAS

ABSTRACT

The CoSiBEA zeolites are prepared by a two-step postsynthesis method which allows to incorporate cobalt in BEA zeolite as isolated tetrahedral Co(II) species. The incorporation of Co ions in vacant T-sites and their reaction with silanol groups are evidenced by XRD and FTIR respectively. It does not generate acidic Brønsted sites as shown by FTIR of adsorbed pyridine. The state of cobalt species is characterized by DR UV–vis and XAS. These techniques allow to show that for low Co content (0.8 wt%) the cobalt is present as lattice tetrahedral Co(II) species. For much higher Co content (11 wt%) mainly extra-lattice octahedral Co(II) species and/or cobalt oxides are evidenced by DR UV–vis spectroscopy. Zeolite with isolated tetrahedral Co(II) species is active in SCR of NO by ethanol with selectivity towards N_2 exceeding 85% for NO conversion from 30 to 70%. When extra-lattice octahedral Co(II) species and/or cobalt oxides appear, the full oxidation of ethanol and NO by dioxygen to CO_2 and NO_2 respectively, are the main reaction pathways. Possible way of the formation of lattice tetrahedral Co(II) species in the BEA structure is proposed.

1. Introduction

It is well known that transition metal ions introduced in pentasil ring zeolites with MOR, MFI and BEA topologies exhibit high activity and selectivity in numerous redox reactions, such as the decomposition of NO [1,2], the ammoxidation of ethane to acetonitrile [3,4] and the selective catalytic reduction (SCR) of NO_x [5–19]. Reaction kinetic studies have shown that the transition metal ions exhibit different activity depending on the location of the metal ions in zeolite structure [2,20]. Thus, the relation between the activity and the location of metal ions in zeolite structure have particular interest in understanding the relation between nature and state of metal species in zeolite structure and the catalytic properties of metal containing zeolites [2,20–27].

Cobalt containing zeolites have been the subject of much interest over the last years [28–37], largely because of their catalytic performance in the selective catalytic reduction of nitrogen oxides by methane [28–33]. Usually, the Co cations are introduced into the zeolite by ion exchange. However, zeolites with transition metal cations incorporated within the lattice exhibit different and very often interesting catalytic properties. Recently [21,38,39], we have shown that it is possible to control an introduction of cobalt in lattice position of BEA zeolite by two-step postsynthesis method and to obtain a CoSiBEA catalyst active in SCR of NO by ethanol.

In this work, we propose the way for incorporation of cobalt in BEA zeolite as isolated tetrahedral Co(II) species and we compare the activity of as obtained CoSiBEA zeolite containing only lattice tetrahedral Co(II) species with that containing mainly extra-lattice octahedral Co(II) species and/or cobalt oxides. The CoSiBEA zeolites with different nature of Co species have been obtained and characterized by macroscopic (chemical analysis, XRD) and molecular (DR UV–vis, XAS spectroscopy) techniques.

2. Experimental

2.1. Catalyst preparation

CoSiBEA zeolites were prepared by the two-step postsynthesis method reported earlier [39–41]. To obtain samples with 0.8 and

* Corresponding author at: UPMC Univ Paris 6, UMR 7609, Laboratoire de Réactivité de Surface, 4 Place Jussieu, 75252 Paris Cedex 05, France.
Fax: +33 1 44 27 60 33.
** Corresponding author. Fax: +48 12 4251923.
E-mail addresses: ncjanas@cyf-kr.edu.pl (J. Janas), stanislaw.dzwigaj@upmc.fr (S. Dzwigaj).

0926-3373/$ – see front matter © 2008 Elsevier B.V. All rights reserved.
doi:10.1016/j.apcatb.2008.11.028

11 Co wt%, 2 g of siliceous BEA zeolite (Si/Al > 1300), obtained by treatment of a tetraethyl ammonium (TEA) BEA zeolite (Si/Al = 11) in a 13 mol L^{-1} HNO_3 solution (4 h, 353 K), were stirred for 24 h at 298 K in aqueous solutions containing 1.2×10^{-3} or 18×10^{-3} mol L^{-1} of $Co(NO_3)_2 \cdot 6H_2O$. Then, the suspensions were stirred for 2 h in air at 353 K until the water was completely evaporated. The solids were washed and then dried in air at 353 K for 24 h. The solids containing 0.8 and 11 Co wt% were labelled $Co_{0.8}$SiBEA and Co_{11}SiBEA respectively. These samples were characterized by different techniques after a particular treatment described in Section 2.2.

2.2. Catalyst characterization

Powder X-ray diffractograms were recorded at room temperature and ambient atmosphere on a Siemens D5000 using the CuK_α radiation (λ = 154.05 pm).

Transmission FTIR spectra of self-supported wafers, with diameter of 12 mm introduced into an *in situ* IR cell equipped with CaF_2 windows, were recorded at room temperature on a Perkin Elmer Spectrum One spectrometer with a resolution of 2 cm^{-1} after calcination at 773 K for 3 h in flowing dry air and then outgassing to 10^{-3} Pa at 573 K. The number of scans was 32. Dehydrated wafers were contacted with gaseous pyridine at room temperature *via* a separate cell containing liquid pyridine. Physisorbed pyridine was outgassed (10^{-3} Pa) for 2 h at 423, 473, 523 and 573 K.

DR UV-vis spectra were recorded at room temperature and ambient atmosphere on a Cary 5E spectrometer equipped with a double integrator with $BaSO_4$ as reference.

X-ray absorption spectra (XAS) were measured on the beam line BL-9A at Photon Factory in the Institute of Materials Structure Science for High Energy Accelerator Research Organization at Tsukuba, Japan (Proposal No. 2007G127). Co K-edge XAFS spectra of $Co_{0.8}$SiBEA sample were measured with a fluorescence mode at room temperature by using ion chamber (100% N_2 diluted (I_0)) and Lytle detector (100% Ar), respectively. The spectra of CoO as reference and Co_{11}SiBEA were measured in transmission mode at room temperature by using two ion chambers (100% N_2 (I_0) and 75% N_2 diluted with Ar (I)). Si(1 1 1) single crystal was used to obtain a monochromatic X-ray beam. Photon energy was calibrated by the characteristic peak found at the low energy side of the edge of the absorption spectrum of Cu foil (8978 eV).

Analyses of EXAFS data were performed using the REX2000 program (Version: 2.5.7; Rigaku Corp.). For EXAFS analyses, the oscillation was first extracted from EXAFS data using a spline smoothing method [42]. The oscillation was normalized by the edge height around 70–100 eV higher than the threshold. The Fourier transformation of k^3-weighted EXAFS oscillation was performed over a k-range of 3.0–13.0 $Å^{-1}$. Inversely Fourier transformed data for each Fourier peak were analyzed by a curve fitting method, using theoretical phase shifts and amplitude functions derived by the FEFF8.2 program [43].

2.3. Catalysis measurements

The activity of catalysts in the SCR of NO by ethanol was measured in a conventional flow Pyrex reactor with internal diameter of 10 mm. The reaction temperature was measured and controlled, with precision of 0.5 K, with the help of two thermocouples: first, inserted in catalyst bed and second, placed inside of electric oven.

The composition of the feed was 1000 ppm NO, 1000 ppm ethanol, the mixture of 2 vol.% O_2 in He with a catalyst volume of 1 ml (~0.52 g) and 10,000 h^{-1} gas hour space velocity. The O_2 and NO were regulated by mass flow controller. Ethanol is introduced as the liquid into the He stream by means of syringe infusion pump provided with 2.5 ml Hamilton syringe and then evaporated in 25 cm long heated stainless pipe.

A gas chromatograph (CHROM-5) provided with TCD and FID detectors was used for analysis of gas phase components. CO_2, NO and C_2H_4 were separated with a 8 ft × 1/8 in. nickel HayeSep R column (Alltech) at 333 K. O_2, N_2 and CO were separated on a SS 2 m × 3 mm MS 5A column (Supelco) at the same temperature. Ethanol and other organic compounds (mainly ethylene, acetaldehyde, acetic acid, acetonitrile, and – in minor quantities – esters and other hydrocarbons) were separated with a FID detector and 2 m × 3 mm glass columns: 10% SP-1000 on 80/100 Supelcort and 10% SP-2100 on 100/120 Supelcort, heated from 333 to 393 K.

The calculations were performed with the CHROMA 2000 computer analytical program. The NO and C_2H_4 concentrations were additionally monitored by means of Photovac S 50 GC equipped with PID 10.6 eV detector. The NO and ethylene concentrations were additionally measured by means of a Photovac 10S50 GC with KCl-alumina column (at 313 K) provided with a photoionization detector. Gas samples are taken from the inlet and outlet of chemical reactor by means of Hamilton analytical syringes (1 ml for TCD, 100 μl for FID and 10 μl for PID analysis) and injected into GC.

Parallel to the GC analysis, the O_2, NO, NO_2 and CO concentrations were monitored with a MADUR GA-60 flue gas analyzer provided with electrochemical sensor. The presence among reaction products of active intermediates such as HCN, NH_3 and HNCO was detected by a FTIR multichannel GASMET DX-4000 gas analyzer (resolution: 7.72 cm^{-1}, optical length: 500 cm, scan time: 60 s).

Before catalytic tests, the samples were heated up to 523 K in oxygen/helium mixture and then NO and ethanol vapour streams were switched on. The standard conditions were: 2 h catalytic runs at 523–623 K and 1 h runs at higher reaction temperature (NO_x and CO_x concentrations at the reactor outlet were continuously monitored to check if pseudo steady-state conditions were established). The reaction temperature was increased every 50 K interval up to 773 K and then lowered in the same way to 523 K. In the case of NO conversion or product selectivity measurements, the heating sequence is repeated to obtain real steady-state reaction conditions in the whole reaction temperature range. Only for NO oxidation experiments in absence of ethanol, heating of the catalysts in a mixture containing 2 vol.%. O_2 in He at 723 K for 1 h was necessary in order to obtain a reproducible activity.

All conversion and selectivity values used in the text were defined and calculated in standard manner and presented in mol.%. Because of difficulties with the straight determination of N_2 concentration at the reactor outlet (taking into consideration the average concentration of this compound at the reactor outlet and inevitable error connected with the syringe operations), the selectivity to N_2 is determined as follows:

$$S_{N_2} = 100 - (S_{NO_2} + S_{N_2O} + S_{NH_3} + S_{OrgN}), \quad [\%]$$

where: S_{NO_2}, S_{N_2O} and S_{NH_3} selectivity into the NO_2, N_2O and ammonia, respectively and S_{OrgN} is the sum of selectivities into nitrogen-containing organic compounds (in the case of Co_xSiBEA zeolites there is practically only acetonitrile and traces of HCN among the N-containing organic products).

3. Results and discussion

3.1. XRD and FTIR evidence for incorporation of cobalt into lattice sites of BEA zeolite

3.1.1. X-ray diffraction analysis

As shown earlier [21,38,39], the crystallinity of BEA zeolite is preserved upon dealumination and introduction of cobalt ions in

SiBEA zeolite, and the samples do not show any evidence of extra-lattice crystalline compounds or long-range amorphization of the zeolite. The d_{302} spacing related to the main peak near 22.6° increases from 3.912 Å (SiBEA) to 3.939 for $Co_{0.8}$SiBEA and 3.942 Å for Co_{11}SiBEA which indicates expansion of the matrix [44,45]. Absence of any diffraction lines of Co_2O_3 or CoO crystals indicates a well dispersion of cobalt species in both CoSiBEA samples. However, that absence of diffraction lines related to Co oxides could be also referred to small particle size, in particular for Co_{11}SiBEA with high Co content.

3.1.2. FTIR spectroscopy and pyridine adsorption

The treatment of AlBEA zeolite with aqueous HNO_3 solution involves the elimination of Al atoms from the framework (Scheme 1, reaction (1)) as evidenced by the disappearance of IR bands at 3781, 3665 and 3609 cm^{-1} attributed to AlO–H and Al–O(H)–Si groups, respectively (Fig. 1), in line with earlier investigations [40,41,46,47]. The appearance of narrow bands at 3736 and 3710 cm^{-1} related to isolated silanol groups and of a broad band at 3520 cm^{-1} due to H-bonded SiOH groups in SiBEA reveals the presence of vacant T-sites associated with silanol groups (Scheme 1, reaction (1)), in line with earlier reports [40,41,46].

The incorporation of Co into SiBEA zeolite leading to $Co_{0.8}$SiBEA induces a reduction of intensity of these bands, in particular that at 3520 cm^{-1} corresponding to H-bonded SiOH groups as shown in Fig. 1, in the same way as observed earlier for the incorporation of V into SiBEA [40,41], suggesting that silanol groups are consumed in the reaction with cobalt precursor and a tetrahedral Co(II) species are formed (Scheme 1, reaction (2)).

To check the acidity of $Co_{0.8}$SiBEA, pyridine is adsorbed on the dehydrated sample at room temperature and FTIR spectra recorded after desorption of pyridine at different temperatures (Fig. 2). The pyridinium cations IR bands are not observed on the dehydrated $Co_{0.8}$SiBEA, indicating that Brønsted acidic sites are not present. It suggests that two SiOH groups present in environment of Co(II) site are not in strong interaction with cobalt ion (Scheme 1, tetrahedral Co(II) site) and have not got acidic character. Only the bands at 1609, 1598, 1578, 1492 and 1448 cm^{-1} are observed (Fig. 2, spectrum b) corresponding to pyridine interacting with Lewis acidic sites and/or physisorbed pyridine, in line with earlier report [48–50]. The intensities of these bands decrease with increasing the temperature desorption as shown by Fig. 2 (spectra c–e).

3.2. The state of cobalt determined by DR UV–vis and XAS

3.2.1. Diffuse reflectance UV–vis spectroscopy

The $Co_{0.8}$SiBEA exhibit three DR UV–vis bands at about 537, 590 and 647 nm (Fig. 3) assigned to isolated tetrahedral Co(II) species and attributed to $^4A_2 \rightarrow {}^4T_1$ (^4P), $^4A_2 \rightarrow {}^4T_1$ (^4F) and $^4A_2 \rightarrow {}^4T_2$ transitions respectively, in line with earlier studies on Co-MFI and CoAPO-5 [51–56]. The broad band around 300 nm is difficult to assign although it may be likely associated with oxygen-to-metal charge transfer (CT) transition [51,57,58].

As already reported [39], the presence of tetrahedral Co^{2+} in CoSiBEA with low Co content is confirmed by a broad, axially symmetric EPR signal with effective g components of $g_{\perp} = 5.4$ and $g_{//} \sim 2.7$ observed at 4 K and attributed to tetrahedral high-spin Co^{2+} ($S = 3/2$) ion [39,57,59,60].

For much higher cobalt content (11 Co wt%), the DR UV–vis bands at ~ 516, 444 and 478 nm appear (Fig. 3, Co_{11}SiBEA sample) assigned to octahedral Co(II) species ($3d^7$ configuration) and/or cobalt oxides, in line with earlier report on Co-MFI zeolite [61,62].

3.2.2. XANES

Fig. 4 shows the Co K-edge XANES spectra of CoO, $Co_{0.8}$SiBEA and Co_{11}SiBEA. The pre-edge peak at 7709 eV is attributed to the 1 s–3d transition and the white line around 7720 eV to the 1 s–4p transition. The intensity of pre-edge peak is related to the coordination environment state of the cobalt [63–65]. However, it is generally weak as well as for Fe and Ni absorption, as it is shown, for example, for framework Co(II) on CoAPO-5 by Thomson et al. [57].

The intensity of pre-edge of $Co_{0.8}$SiBEA is higher than that of CoO, where all cobalt species are located in octahedral site. The pre-edge peak position of Co_{11}SiBEA is almost similar to that of CoO. The width of white line around 7720 eV of $Co_{0.8}$SiBEA sample is broader than that of Co_{11}SiBEA sample. Moreover, in the case of Co_{11}SiBEA and CoO, the broad band around 7735–7740 eV was observed, whereas $Co_{0.8}$SiBEA sample did not show this band, indicating that the local environment of cobalt species in $Co_{0.8}$SiBEA is different from that of Co_{11}SiBEA and CoO.

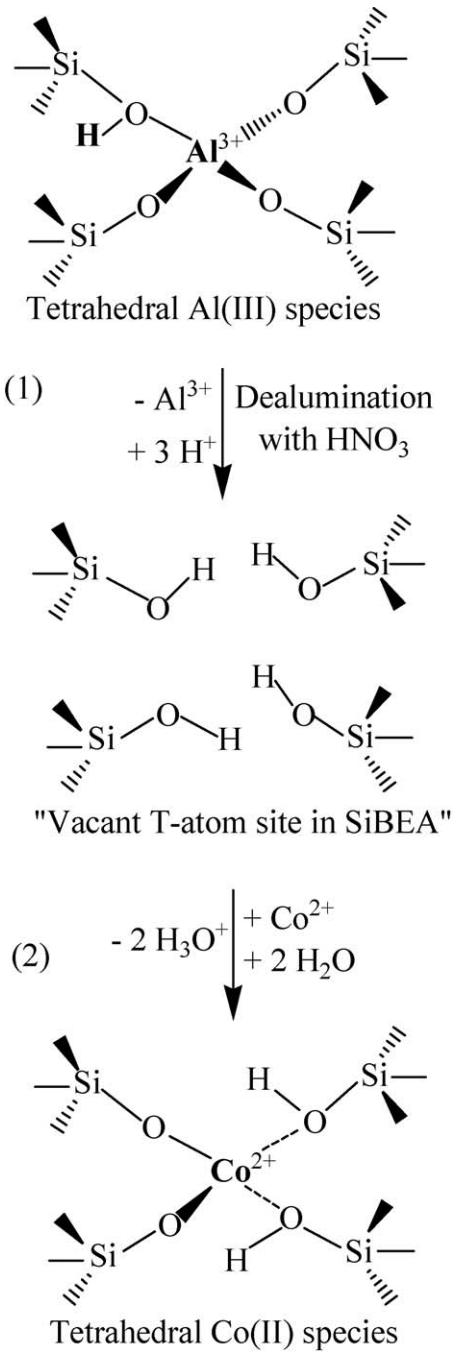

Scheme 1.

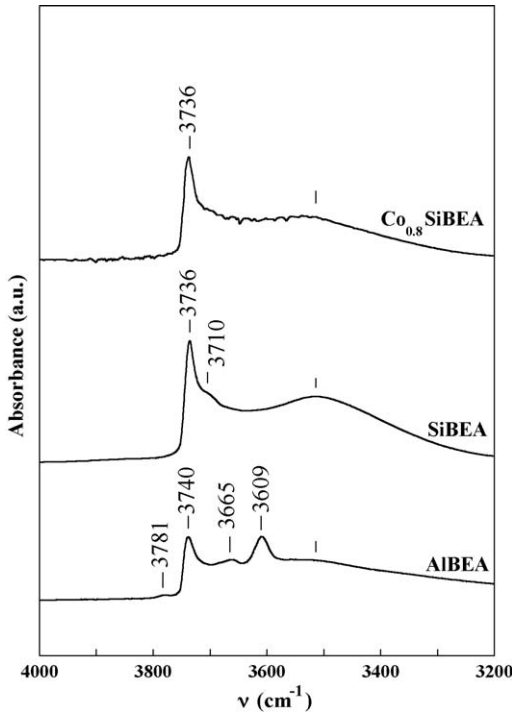

Fig. 1. FTIR of AlBEA, SiBEA, $Co_{0.8}$SiBEA recorded at room temperature after calcination at 773 K for 3 h in flowing air and then outgassing at 573 K under vacuum up to 10^{-3} Pa.

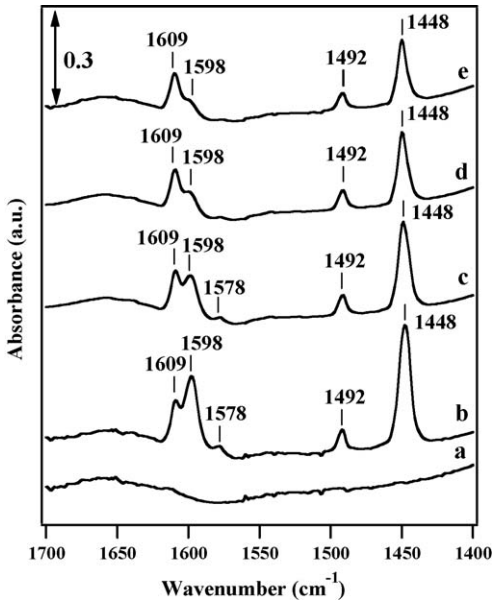

Fig. 2. FTIR spectra recorded at room temperature of (a) $Co_{0.8}$SiBEA zeolite after calcination at 773 K, 3 h in flowing air, outgassing at 10^{-3} Pa for 2 h at 573 K, adsorption of pyridine at room temperature and desorption of pyridine at (b) 423 K, (c) 473 K, (d) 523 K and (e) 573 K.

The Co K-edge XANES spectra confirm the DR UV–vis observations and suggest that the tetrahedral Co(II) species are present in $Co_{0.8}$SiBEA, whereas the octahedral Co(II) species are mainly present in Co_{11}SiBEA similarly as for CoO.

3.2.3. EXAFS

Fig. 5 shows the Fourier transform of k^3-weighted Co K-edge EXAFS spectra of reference compound (CoO) and $Co_{0.8}$SiBEA and Co_{11}SiBEA samples. For CoO (rock-salt type) structure, a peak at 1.7

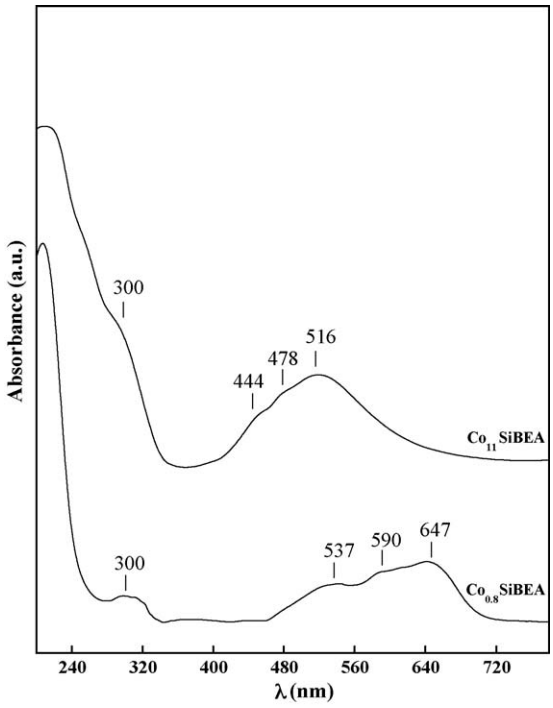

Fig. 3. DR UV–vis spectra recorded at room temperature of $Co_{0.8}$SiBEA and Co_{11}SiBEA.

(without phase shift correction) appears which is due to the presence in the first shell of Co(II) of six oxygen neighbours. The peak at 2.7 Å is assigned to Co–O–Co species. The Fourier transforms of k^3-weighted Co K-edge EXAFS spectra of $Co_{0.8}$SiBEA and Co_{11}SiBEA

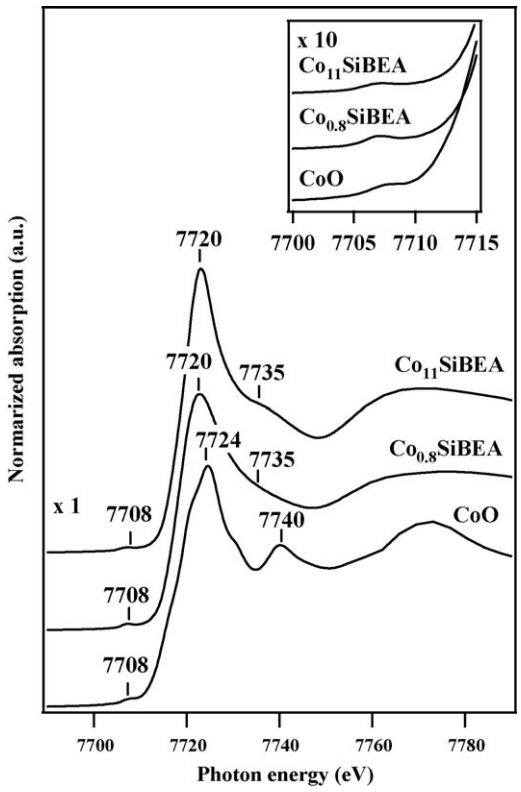

Fig. 4. Co K-edge XANES spectra recorded at room temperature of reference compound (CoO) and $Co_{0.8}$SiBEA and Co_{11}SiBEA. The insets for CoO, $Co_{0.8}$SiBEA and Co_{11}SiBEA correspond to a magnification of 10.

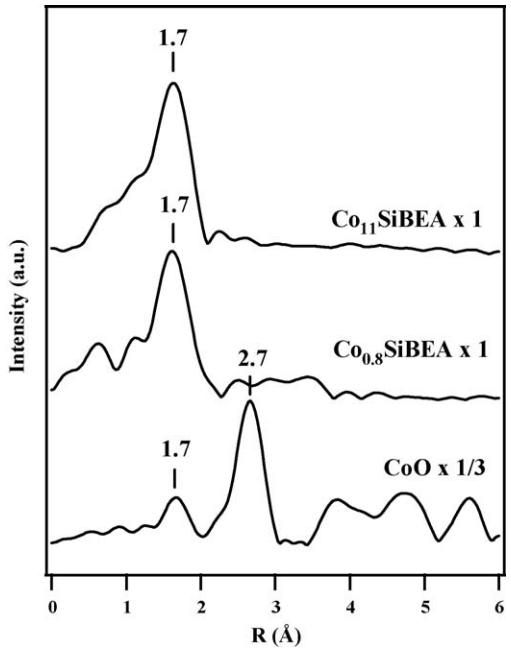

Fig. 5. Fourier transforms of k^3-weighted Co K-edge EXAFS spectra recorded at room temperature of reference compound (CoO) and $Co_{0.8}$SiBEA and Co_{11}SiBEA.

Table 1
Curve fitting results of Co K-edge EXAFS for $Co_{0.8}$SiBEA and Co_{11}SiBEA and CoO reference[a,b].

Sample	C.N.	R (Å)	σ (Å)	ΔE_0 (eV)	R_f (%)
$Co_{0.8}$SiBEA	3.6 ± 0.6	2.06 ± 0.01	0.08 ± 0.02	2.5 ± 2.7	8.9
Co_{11}SiBEA	4.5 ± 0.8	2.08 ± 0.01	0.08 ± 0.02	1.5 ± 2.8	6.3
CoO[c]	6	2.13	–	–	–
	12	3.02			

[a] C.N., coordination number; R, bond length; ΔE_0, difference in the origin of photoelectron energy between the reference and the sample; σ, Debye-Waller factor; R_f, residual factor.
[b] Inverse Fourier range ΔR = 1.1–2.0 Å, fitting range Δk = 3.8–13.4 Å^{-1}.
[c] Obtained from crystallographic data.

show the peak at 1.7 Å due to the presence in the first shell of Co(II) of four and/or six oxygen neighbours. A lack of peak around 2.7 Å in both $Co_{0.8}$SiBEA and Co_{11}SiBEA indicates that even for the latter sample the amount of polynuclear Co(II) (Co–O–Co) species is not important and/or they are well dispersed in zeolite structure.

Table 1 shows the results of curve fitting analysis for first coordination sphere of $Co_{0.8}$SiBEA and Co_{11}SiBEA. The coordination number of Co–O bond of $Co_{0.8}$SiBEA is about 3.6, indicating that the tetrahedral Co(II) species is stabilized in $Co_{0.8}$SiBEA. On the contrary, the coordination number of Co–O bond of Co_{11}SiBEA is higher than that of $Co_{0.8}$SiBEA (about 4.5). This suggests that a part of Co(II) species is present in higher than tetrahedral coordination. On the basis of XANES and EXAFS spectra, a highly dispersed tetrahedral Co(II) species is considered to be stabilized in $Co_{0.8}$SiBEA. In the case of Co_{11}SiBEA, cobalt is present as a mixture of tetrahedral and octahedral Co(II) species.

XRD, DR UV–vis and XAS results show that for low Co content cobalt is incorporated into the BEA lattice as tetrahedral Co(II) species (Scheme 1, reaction (2)). For much higher Co content (11 wt%), mainly octahedral Co(II) species and/or cobalt oxides appear in extra-lattice position.

3.3. The role of tetrahedral Co(II) sites in SCR of NO by ethanol

Fig. 6 compares the conversion of ethanol in SCR of NO. As we can see, conversion of ethanol on both samples is very high and

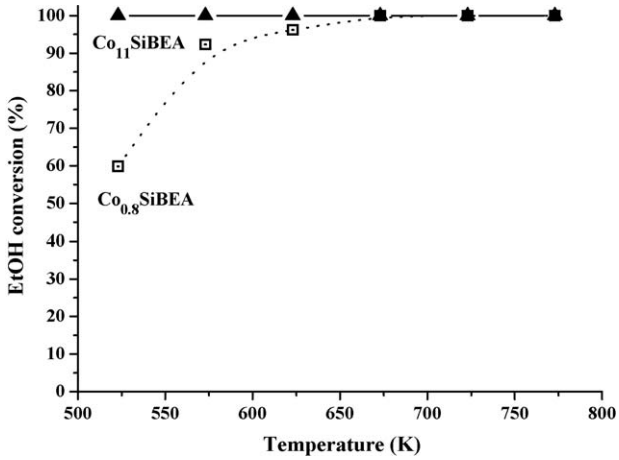

Fig. 6. Temperature-dependence of ethanol conversion in SCR of NO by ethanol on $Co_{0.8}$SiBEA and Co_{11}SiBEA.

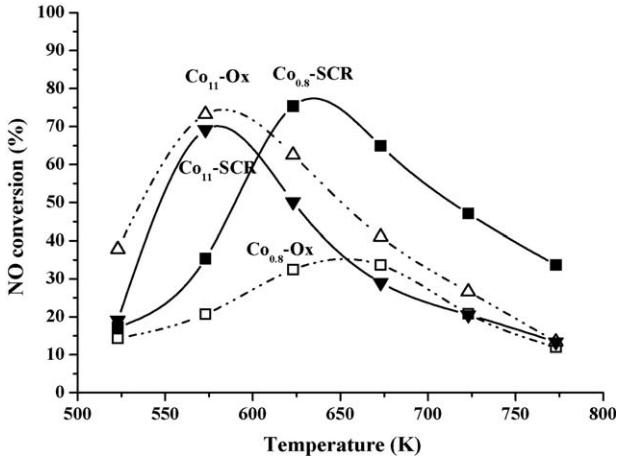

Fig. 7. Temperature-dependence of NO conversion in SCR of NO by ethanol on $Co_{0.8}$SiBEA and Co_{11}SiBEA.

reaches 100% already at 550 K for Co_{11}SiBEA and above 625 K for $Co_{0.8}$SiBEA. The conversions of NO in SCR of NO by ethanol are relatively high for both samples and reaches 70% for Co_{11}SiBEA at temperature of 575 K (Fig. 7) (marked as Co_{11}-SCR) and about 80% for $Co_{0.8}$SiBEA (marked as $Co_{0.8}$-SCR). It is clearly shown that the NO conversion in NO oxidation reaction in the absence of ethanol for the sample with high Co content (Co_{11}SiBEA) is much higher than that observed for the sample with low Co content ($Co_{0.8}$SiBEA), marked on the Fig. 7, respectively, as Co_{11}-Ox and $Co_{0.8}$-Ox. Moreover, for Co_{11}SiBEA, NO conversion in NO oxidation reaction is even higher than the NO conversion in SCR of NO by ethanol. It suggests that the presence of extra-lattice octahedral Co(II) species enhance the activity of CoSiBEA zeolites in full oxidation of ethanol to CO_2 and NO to NO_2.

Figs. 7 and 8 show that $Co_{0.8}$SiBEA with lattice tetrahedral Co(II) species is active in SCR of NO with ethanol over a wide temperature range. For this sample, the main reaction route is the reduction of NO into N_2. The selectivity toward N_2 exceeds 85% for NO conversion from 30 to 70%. For this sample, the selectivity toward NO_2 is lower than 10% in the reaction temperature range between 525 and 675 K (Fig. 9).

Above 650 K, ethanol conversion reaches 100% for $Co_{0.8}$SiBEA sample (Fig. 6) and NO conversion (Fig. 7) and selectivity toward N_2 (Fig. 8) decrease. Above this temperature, the amounts of mild oxidation products (ethene, CO or other organic products) are very low, more NO_2 appears and its amount increases with tempera-

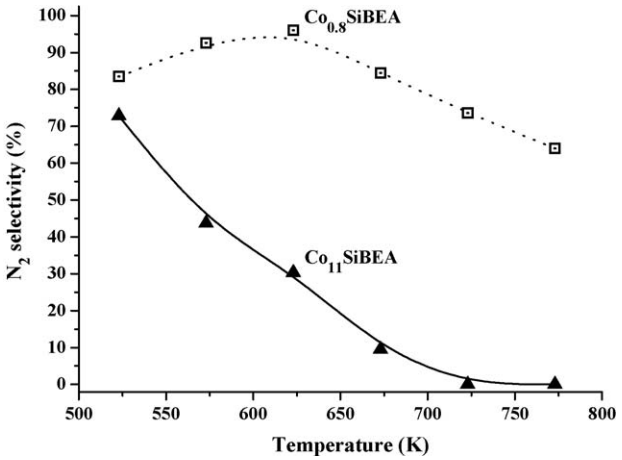

Fig. 8. Temperature-dependence of N_2 selectivity in SCR of NO by ethanol on $Co_{0.8}$SiBEA and Co_{11}SiBEA.

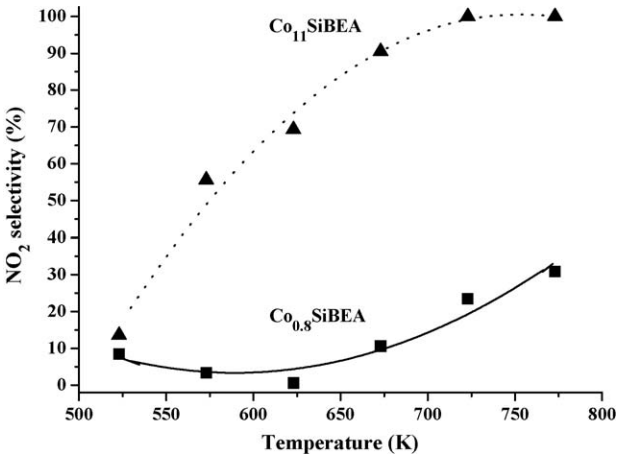

Fig. 9. Temperature-dependence of NO_2 selectivity in SCR of NO by ethanol on $Co_{0.8}$SiBEA and Co_{11}SiBEA.

ture. However, for $Co_{0.8}$SiBEA containing only isolated tetrahedral Co(II) species, the relatively low level of NO oxidation into NO_2 is observed for comparison with Co_{11}SiBEA (Fig. 9).

With a further increase of the reaction temperature, the straight oxidation reaction of ethanol and other oxygenates which proceeds is parallel to the SCR of NO causes that their concentration in gas phase diminishes [66]. Depending on the rate constants and activation energy of both processes, conversion of NO and N_2 selectivity reach a maximum and then decrease.

The volcano-like shape of NO conversion during the SCR of NO observed for $Co_{0.8}$SiBEA and Co_{11}SiBEA catalysts is typical of various catalytic systems and different organic molecules used as reducing agent. The similar shape resembles the temperature-dependence of the NO oxidation reaction [30,67]. The analysis of the NO conversion shape points out that in the case of Co_{11}SiBEA it follows the thermodynamic limitation in the high temperature range, what is due to the total oxidation of ethanol and the all organic intermediates. Thus, the NO–NO_2 equilibration determines the NO conversion level and NO_2 yield. At the same reaction temperatures, NO conversion level on $Co_{0.8}$SiBEA is much higher than it could be expected from thermodynamics. The unusual behaviour in SCR leading to the high NO conversion and NO_2 yield values above 773 K was earlier described [68] but on $Co_{0.8}$SiBEA the NO_2 yield (Fig. 11) follows the thermodynamic limitation indicating, that the high NO conversion is due to the surface

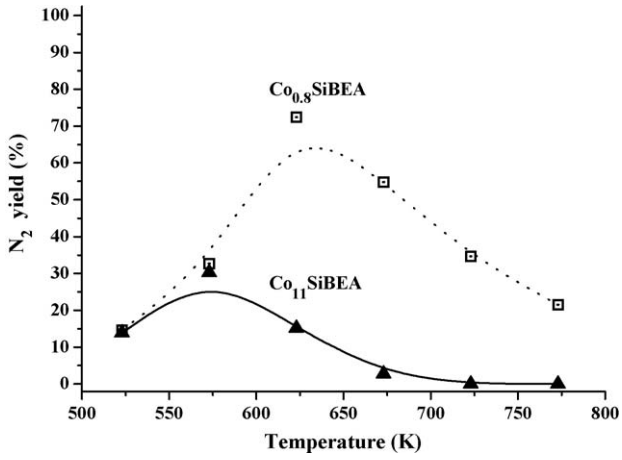

Fig. 10. Temperature-dependence of N_2 yield in SCR of NO by ethanol on $Co_{0.8}$SiBEA and Co_{11}SiBEA.

reaction between the adsorbed NO_x and some organic active species.

Co_{11}SiBEA with extra-lattice octahedral Co(II) species and/or cobalt oxides is characterized by the high selectivity toward NO_2 (Fig. 9) and consequently, the low selectivity toward N_2 in comparison with $Co_{0.8}$SiBEA (Fig. 8). It evidences that Co_{11}SiBEA is much less active than $Co_{0.8}$SiBEA in SCR of NO with maximum N_2 yield lower than 25% at 575 K and close to zero above 700 K (Fig. 10) and much more active in full oxidation of NO toward NO_2 with maximum NO_2 yield close to 35% at 600 K (Fig. 11) and of ethanol toward CO_2 with CO_2 selectivity higher than 80% in 525–775 K temperature range (Fig. 12).

These results show that the tetrahedral Co(II) species are responsible for the activity in SCR of NO by ethanol and selectivity toward N_2 while octahedral Co(II) species and/or cobalt oxides present in Co_{11}SiBEA are detrimental for the N_2 selectivity.

We suggest, that the decrease of selectivity toward N_2 at higher temperature particularly on catalysts containing mainly extra-lattice octahedral Co(II) species and/or cobalt oxides (Co_{11}SiBEA sample) is related to the depletion of organic mild oxidation products in the reaction zone as a result of full oxidation of ethanol by O_2. It is evidenced, that extra-lattice cobalt oxides enhance of the activity of Co_{11}SiBEA zeolite in full oxidation of ethanol to CO_2 (Fig. 12) and also in oxidation of NO to NO_2, (Fig. 9) in particular at high temperatures.

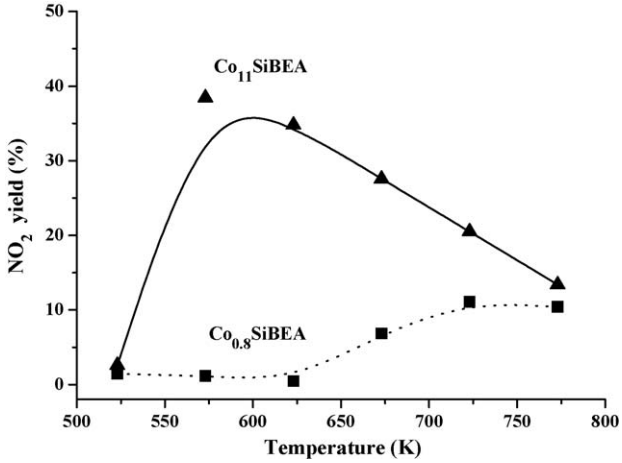

Fig. 11. Temperature-dependence of NO_2 yield in SCR of NO by ethanol on $Co_{0.8}$SiBEA and Co_{11}SiBEA.

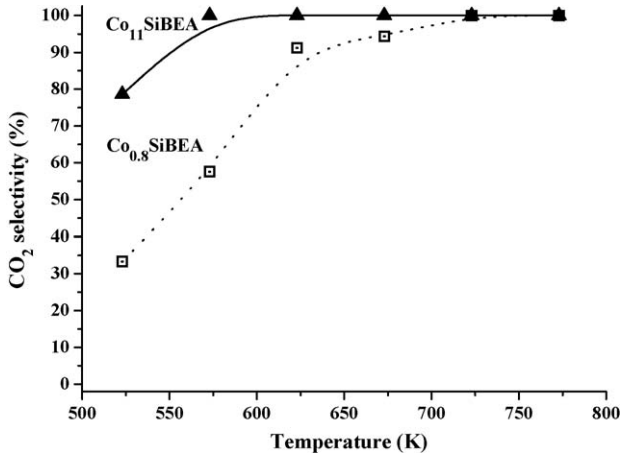

Fig. 12. Temperature-dependence of CO_2 selectivity in SCR of NO by ethanol on $Co_{0.8}$SiBEA and Co_{11}SiBEA.

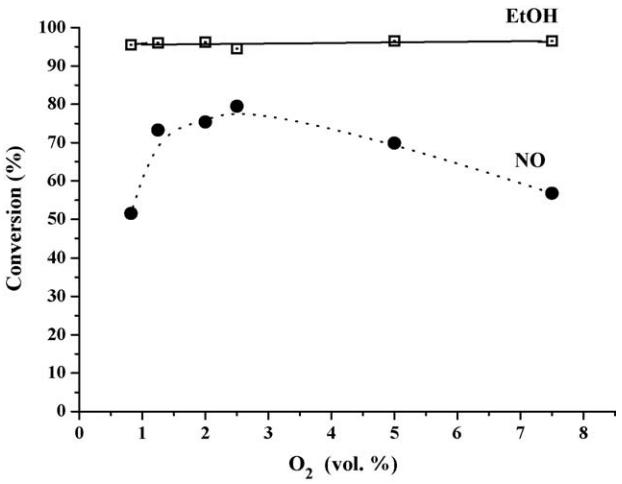

Fig. 13. Dependence of ethanol and NO conversions on O_2 concentration in SCR of NO by ethanol on $Co_{0.8}$SiBEA.

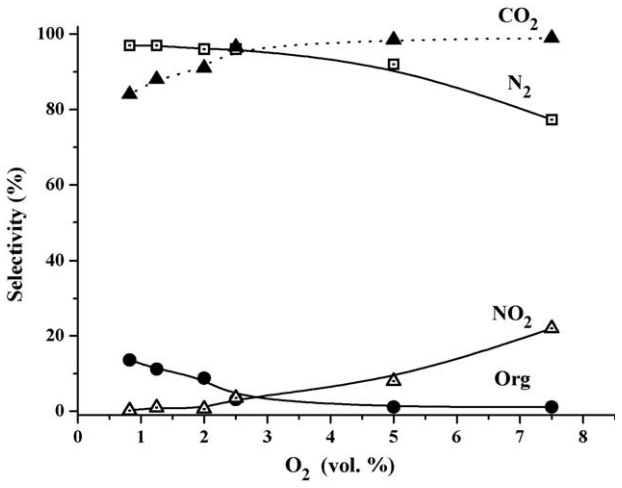

Fig. 14. Dependence of products selectivities on O_2 concentration in SCR of NO by ethanol on $Co_{0.8}$SiBEA.

This conclusion is very close to that formulated in [69], where the active sites for NO reduction over Fe-ZSM-5 were discussed. Nevertheless, it must be kept in mind that indication of the active sites responsible for the catalytic activity in SCR of NO of Me-zeolites, including Fe-BEA and Fe-ZSM-5, presented in literature [15–19,70] refer to the Al-containing zeolite with different types of iron species: isolated lattice and extra-lattice Fe species, Fe oligomers and Fe oxides. These various Fe species have been discussed as a potential sites of SCR of NO in the presence of different reducing agents.

However, not only these Fe species are possible active sites in the Fe-exchanged zeolite. We have to take in account the lattice and extra-lattice Al species as well as transition metal impurities which may be also involved as active sites as it has recently been evidenced for BEA, MOR and MFI zeolites by Dzwigaj et al. [26]. In the latter paper, for sake of comparison, partly and completely dealuminated BEA zeolites, containing small amounts or no iron impurities as well as MOR and MFI zeolites were also investigated.

Moreover, in the preliminary investigation on SCR of NO by ethanol on FeSiBEA catalysts prepared by postsynthesis method recently reported by Dzwigaj et al. [21], the role of different Fe species was elucidated and the conclusions are very similar to those pointed out in this work.

The data reported here show that the activity in NO oxidation to NO_2 does not necessarily imply SCR activity, as it was postulated earlier by several authors [67,71]. The less NO oxidation is favored, the more SCR of NO toward N_2 on CoSiBEA occurs. According to our previous work [72] and literature data [66,67], it is likely that the reaction mechanism involves the preliminary adsorption of NO that is oxidized by O_2 forming an adsorbed NO_x species ($x = 2,3$) bound to Co(II) center. Lattice tetrahedral Co(II) species present in $Co_{0.8}$SiBEA zeolite could activate ethanol by a abstracting a hydrogen atom and then forming an oxygenated intermediate. This active intermediate is probably responsible for SCR of NO toward N_2 [73].

We would like to mention here that we have also performed SCR of NO with higher O_2 concentration in the mixture with He than 2 vol.%. However, we have decided to use the mixture of 2 vol.% O_2 in He in major part of our work because the more pronounced differences in catalytic activity and product selectivities observed for CoSiBEA samples for this oxygen concentration.

The results with various O_2 concentrations are presented on the Figs. 13 and 14. They show that the increase of O_2 concentration in the feed does not change significantly the trend observed in this work. The conversion of ethanol as well as selectivity into Org ($CO + C_2H_4$) is not changed, in contrast, NO conversion and selectivity into N_2 diminished slightly along with increase of O_2 concentration.

4. Conclusions

The $Co_{0.8}$SiBEA and Co_{11}SiBEA zeolites with 0.8 and 11 Co wt% are prepared by a two-step postsynthesis method. It allows to incorporate cobalt in BEA zeolite mainly as isolated lattice tetrahedral Co(II) species for $Co_{0.8}$SiBEA and as extra-lattice octahedral Co(II) species for Co_{11}SiBEA. The incorporation of Co ions in vacant T-sites and their reaction with silanol groups are evidenced by XRD and FTIR respectively. It does not generate acidic Brønsted sites as shown by FTIR of pyridine adsorption.

The state of cobalt species is characterised by DR UV–vis and XAS. The combined use of these techniques allows to show that for low Co content (0.8 wt%) the cobalt is present as the distorted tetrahedral Co(II) species. For much higher Co content (11 wt%) additional extra-lattice octahedral Co(II) species and/or cobalt oxides are evidenced by DR UV–vis spectroscopy.

The catalytic activity of CoSiBEA strongly depends on the nature and environment of Co species. Zeolite with lattice tetrahedral Co(II) species is active in SCR of NO by ethanol with selectivity towards N_2 exceeding 85% for NO conversion from 30 to 70%. When

additional extra-lattice octahedral Co(II) species and/or cobalt oxides appear, the full oxidation of ethanol and NO by dioxygen to CO_2 and NO_2 respectively, are the main reaction pathways. Possible way of the formation of lattice tetrahedral Co(II) species in the BEA structure is proposed.

Acknowledgments

S.D. gratefully acknowledges the CNRS (France) for financial support as Assistant Researcher.

References

[1] M. Iwamoto, H. Yahiro, K. Tanda, N. Mizuno, Y. Mine, J. Phys. Chem. 95 (1991) 3727.
[2] B. Wichterlova, J. Dedecek, Z. Sobalik, A. Vondrova, K. Klier, J. Catal. 169 (1997) 194.
[3] Y. Li, J.N. Armor, J. Chem. Soc., Chem. Commun. (1997) 2013.
[4] Y. Li, J.N. Armor, J. Catal. 173 (1998) 511.
[5] M. Iwamoto, H. Yahiro, Catal. Today 22 (1994) 5.
[6] M. Iwamoto, T. Zengyo, A.M. Herdandez, H. Araki, Appl. Catal. B 17 (1998) 259.
[7] C.N. Costa, T. Anastasiadou, A.M. Efstathiou, J. Catal. 194 (2000) 250.
[8] M. Shelef, Chem. Rev. 95 (1995) 209.
[9] M. Iwamoto, Catal. Today 29 (1996) 29.
[10] A.W. Aylor, S.C. Larsen, J.A. Reimer, A.T. Bell, J. Catal. 157 (1995) 592.
[11] Y. Li, J.N. Armor, Appl. Catal. B 5 (1995) 257.
[12] B.J. Adelman, T. Beutel, G.D. Lei, W.M.H. Sachtler, J. Catal. 158 (1996) 327.
[13] H.H. Chen, S.C. Shen, X. Chen, S. Kawi, Appl. Catal. B 50 (2004) 37.
[14] B. Wichterlova, Z. Sobalik, J. Dedecek, Appl. Catal. B 41 (2003) 97.
[15] M. Schwidder, S. Heikens, A. De Toni, S. Geisler, M. Berndt, A. Brueckner, W. Gruenert, J. Catal. 259 (2008) 96.
[16] M. Schwidder, M. Santhosh Kumar, U. Bentrup, J. Perez-Ramirez, A. Brueckner, W. Gruenert, Micropor. Mesopor. Mater. 111 (2008) 124.
[17] M. Santhosh Kumar, M. Schwidder, W. Gruenert, U. Bentrup, A. Brueckner, J. Catal. 239 (2006) 173.
[18] R. Burch, S. Scire, Appl. Catal. B 3 (1994) 295.
[19] R. Burch, S. Scire, Catal. Lett. 27 (1994) 177.
[20] D. Kaucky, A. Vondrova, J. Dedecek, B. Wichterlova, J. Catal. 194 (2000) 318.
[21] S. Dzwigaj, J. Janas, T. Machej, M. Che, Catal. Today 119 (2007) 133.
[22] S. Dzwigaj, I. Gressel, B. Grzybowska, K. Samson, Catal. Today 114 (2006) 237.
[23] S. Dzwigaj, M. Che, B. Grzybowska, I. Gressel, K. Samson, Stud. Surf. Sci. Catal. 172 (2007) 385.
[24] J. Perez-Ramirez, J.C. Groen, A. Bruckner, M.S. Kumar, U. Bentrup, M.N. Debbagh, L.A. Villaescusa, J. Catal. 232 (2005) 318.
[25] P. Balle, B. Geiger, S. Kureti, Appl. Catal. B 85 (2009) 109.
[26] S. Dzwigaj, J. Janas, W. Rojek, L. Stievano, F.E. Wagner, F. Averseng, M. Che, Appl. Catal. B 86 (2009) 45.
[27] G. Busca, L. Lietti, G. Ramis, F. Berti, Appl. Catal. B 18 (1998) 1.
[28] Y. Li, J.N. Armor, Appl. Catal. B 1 (1992) L31.
[29] Y. Li, J.N. Armor, J. Catal. 150 (1994) 376.
[30] Y. Traa, B. Burger, J. Weitkamp, Micropor. Mesopor. Mater. 30 (1999) 3.
[31] X. Wang, H.Y. Chen, W.M.H. Sachtler, J. Catal. 19 (2001) 281.
[32] L.J. Lobree, A.W. Aylor, J.A. Reimer, A.T. Bell, J. Catal. 169 (1997) 188.
[33] T. Beutel, B.J. Adelman, W.M.H. Sachtler, Appl. Catal. B 9 (1996) L1.
[34] K. Hadjiivanov, B. Tsyntsarski, T. Nikolova, Phys. Chem. Chem. Phys 1 (1999) 4521.
[35] M.C. Campa, S. de Rossi, G. Ferraris, V. Indovina, Appl. Catal. B 8 (1996) 315.
[36] K. Hadjiivanov, M. Mihaylov, Chem. Commun. (2004) 2200.
[37] M. Inaba, Y. Kintaichi, M. Haneda, H. Hamada, Catal. Lett. 39 (1996) 269.
[38] A. Mihajlova, K. Hadjiivanov, S. Dzwigaj, M. Che, J. Phys. Chem. B 110 (2006) 19530.
[39] S. Dzwigaj, M. Che, J. Phys. Chem. B 110 (2006) 12490.
[40] S. Dzwigaj, M.J. Peltre, P. Massiani, A. Davidson, M. Che, T. Sen, S. Sivasanker, J. Chem. Soc., Chem. Commun. (1998) 87.
[41] S. Dzwigaj, P. Massiani, A. Davidson, M. Che, J. Mol. Catal. 155 (2000) 169.
[42] J.W. Cook, D.E. Sayers, J. Appl. Phys. 52 (1981) 5024.
[43] A.L. Ankudinov, B. Ravel, J.J. Rehr, S.D. Conradson, Phys. Rev. B 58 (1998) 7565.
[44] M.A. Camblor, A. Corma, J. Perez-Pariente, Zeolites 13 (1993) 82.
[45] E.P. Reddy, L. Davydov, G. Smirniotis, J. Phys. Chem. B 106 (2002) 3394.
[46] S. Dzwigaj, M. Matsuoka, R. Franck, M. Anpo, M. Che, J. Phys. Chem. B 102 (1998) 6309.
[47] S. Dzwigaj, M. Matsuoka, M. Anpo, M. Che, J. Phys. Chem. B 104 (2000) 6012.
[48] G. Centi, G. Gollinetti, G. Busca, J. Phys. Chem. 94 (1990) 6813.
[49] G. Busca, G. Centi, F. Tifiro, Y. Lorenzelli, J. Phys. Chem. 90 (1986) 1337.
[50] H. Knözinger, Adv. Catal. 25 (1976) 184.
[51] B.M. Weckhuysen, A.A. Verberckmoes, M.G. Uytterhoeven, F.E. Mabbs, D. Collison, E. de Boer, R.A. Schoonheydt, J. Phys. Chem. B 104 (2000) 37.
[52] B.M. Weckhuysen, R.R. Rao, J.A. Martens, R.A. Schoonheydt, Eur. J. Inorg. Chem. (1999) 565.
[53] M. Hartmann, L. Kevan, Chem. Rev. 99 (1999) 635.
[54] A.A. Verberckmoes, B.M. Weckhuysen, R.A. Schoonheydt, Micropor. Mesopor. Mater. 22 (1998) 165.
[55] W. Fan, B.M. Weckhuysen, R.A. Schoonheydt, Phys. Chem. Chem. Phys. 3 (2001) 3240.
[56] W. Fan, R. Li, T. Dou, T. Tatsumi, B.M. Weckhuysen, Micropor. Mesopor. Mater. 84 (2005) 116.
[57] S. Thomson, V. Luca, R.F. Howe, Phys. Chem. Chem. Phys 1 (1999) 615.
[58] A. Eldewik, R.F. Howe, Micropor. Mesopor. Mater. 48 (2001) 65.
[59] V. Kurshev, L. Kevan, D.J. Parillo, C. Pereira, G.T. Kokotailo, R.J. Gorte, J. Phys. Chem. 98 (1994) 10160.
[60] C. Borges, M.F. Ribeiro, C. Henriques, J.P. Lourenço, D.M. Murphy, A. Louati, Z. Gabelica, J. Phys. Chem. B 108 (2004) 8.
[61] M. Mhamdi, E. Marceau, S. Khaddar-Zine, A. Ghorbel, M. Che, Y. Ben Taarit, F. Villain, Catal. Lett. 98 (2004) 1.
[62] S.J. Jong, S. Cheng, Appl. Catal. A 126 (1995) 51.
[63] F. Farges, G.E. Bown, J. Rehr, J. Phys. Chem. B 56 (1997) 1809.
[64] F.J. Farges, Non-Cryst. Solids 244 (1999) 25.
[65] T.E. Westre, P. Kennepohl, J.G. Dewitt, B. Hedman, K.O. Hodgson, E.I. Solomon, J. Am. Chem. Soc. 119 (1997) 6297.
[66] R. Burch, J.P. Breen, F.C. Meunier, Appl. Catal. B 39 (2002) 283.
[67] N.W. Cant, I.O.Y. Liu, Catal. Today 63 (2000) 133.
[68] F.C. Meunier, J.P. Breen, V. Zuzaniuk, M. Olsson, J.R.H. Ross, J. Catal. 187 (1999) 493.
[69] M. Schwidder, M. Santhosh Kumar, A. Brückner, W. Grünert, J. Chem. Soc., Chem. Commun. (2005) 805.
[70] L. Čapek, J. Dedeček, B. Wichterlova, J. Catal. 227 (2004) 352.
[71] R. Brosius, J.A. Martens, Topics Catal. 29 (2004) 119.
[72] J. Janas, T. Machej, J. Gurgul, R.P. Socha, M. Che, S. Dzwigaj, Appl. Catal. B 75 (2007) 239.
[73] S. Dzwigaj, J. Janas, J. Gurgul, R.P. Socha, T. Shishido, M. Che, Appl. Catal. B 85 (2009) 131.